

Shocked molecular hydrogen towards the Tornado nebula

J. S. Lazendic^{1,2}, M. Wardle³, M. G. Burton⁴, F. Yusef-Zadeh⁵,
A. J. Green¹ and J. B. Whiteoak⁶

¹ *School of Physics A28, University of Sydney, Sydney NSW 2006, Australia*

² *Harvard-Smithsonian Center for Astrophysics, 60 Garden Street, Cambridge, MA 02138, USA*

³ *Department of Physics, Macquarie University, N SW 2109, Australia*

⁴ *School of Physics, University of New South Wales, Sydney NSW 2052, Australia*

⁵ *Department of Physics and Astronomy, Northwestern University, Evanston, IL 60208, USA*

⁶ *Australia Telescope National Facility, CSIRO, PO Box 76, Epping NSW 1710, Australia*

ABSTRACT

We present near-infrared and millimetre-line observations of the Tornado nebula (G357.7–0.1). We detected 2.12 μm H₂ 1–0 S(1) line emission towards the suspected site of interaction with a molecular cloud revealed by the presence of an OH(1720 MHz) maser. The distribution of the H₂ emission is well correlated with the nonthermal radio continuum emission from the Tornado, and the velocity of the H₂ emission spans over 100 km s^{−1}, which both imply that the H₂ emission is shock excited. We also detected millimetre-lines from ¹²CO and ¹³CO transitions at the velocity of the maser, and mapped the distribution of the molecular cloud in a 2×2 arcmin² region around the maser. The peak of the molecular cloud aligns well with an indentation in the nebula’s radio continuum distribution, suggesting that the nebula’s shock is being decelerated at this location, which is consistent with the presence of the OH(1720 MHz) maser and shocked H₂ emission at that location.

Key words: masers – shock waves – ISM: clouds –ISM: individual: Tornado nebula, G357.7–0.1 - supernova remnants.

1 INTRODUCTION

The inner region of our Galaxy is rich in unusual and unique sources. One such object is the Tornado nebula (G357.7–0.1, MSH 17–39), a peculiar nonthermal source with an axially symmetric morphology. Because of its filamentary structure, steep nonthermal radio spectrum and presence of significant linear polarisation, the Tornado has been classified as a supernova remnant (SNR) (Milne 1979; Clark & Caswell 1976; Shaver et al. 1985a). Its elongated and loop-like structure was suggested to be a result of biconical flows from the progenitor star (Manchester 1987) or an accreting binary system (Helfand & Becker 1985; Becker & Helfand 1985). X-ray emission has been detected from the nebula with the *Advanced Satellite for Cosmology and Astrophysics (ASCA)* (Yusef-Zadeh et al. 2003) and *Chandra X-ray Observatory* (Gaensler et al. 2003). Although the emission from the nebula is most probably thermal, deeper observations are needed to unambiguously establish the nature of X-ray emission.

A compact source, called the ‘Eye’ of the Tornado, located about 30 arcsec west from the Tornado, has been linked to the nebula and suggested to be a high proper-motion pulsar associated with the nebula

(Shull, Fesen, & Saken 1989). However, the source was found to have a flat radio spectrum suggestive of an H II region (Shaver et al. 1985b). Most recently, Burton et al. (2004) found 2.16 μm Br γ emission towards the Eye which peaks at a velocity of around -200 km s^{−1}. These observations imply that the Eye is an isolated core where an embedded massive star is in the process of formation, and it is a foreground object to the Tornado. Hydrogen recombination lines were also detected towards the Eye at radio wavelengths (Brogan & Goss 2003).

OH(1720 MHz) masers have been found at the northwestern tip of the Tornado (Frail et al. 1996; Yusef-Zadeh et al. 1999). When not accompanied by detectable maser emission from the other three OH ground-state transitions at 1612, 1665 and 1667 MHz, the 1720 MHz OH transition is believed to be an indicator of an interaction between SNRs and molecular clouds (e.g. Frail et al. 1996; Green et al. 1997; Lockett, Gauthier & Elitzur 1999; Wardle 1999; Wardle & Yusef-Zadeh 2002). The maser in the Tornado has a velocity of -12.4 km s^{−1}, and if its distance is assumed to be more than a few hundred parsec (avoiding the distance ambiguity), a distance of 11.8 kpc is derived from the Galactic rota-

tion curve (Fich, Blitz, & Stark 1989). This is consistent with 21-cm H I absorption against the Tornado, which places the nebula at a distance greater than 5 kpc (Radhakrishnan et al. 1972). The magnetic field strength towards the OH(1720 MHz) maser, determined from measurements of OH-line Zeeman splitting, is 0.7 mG (Brogan et al. 2000).

We obtained near-infrared (NIR) and millimetre-line observations towards the northwestern part of the Tornado to investigate the implied interaction of the nebula and the surrounding molecular gas. We also obtained archival radio continuum data at 20 cm for a comparison. The observations are described in Section 2 and the results are given in Section 3. The results are discussed in Section 4 and summarized in Section 5.

2 DATA

2.1 UNSWIRF observations

For NIR observations of the Tornado we used the University of New South Wales Fabry-Perot narrow-band tunable filter (UNSWIRF; Ryder et al. 1998) mounted on the 3.9-m Anglo-Australian Telescope during June 1999. The observations were centred near the location of the OH(1720 MHz) maser in the nebula at RA(1950) = $17^{\text{h}} 36^{\text{m}} 55^{\text{s}}.4$, Dec.(1950) = $-30^{\circ} 56' 1''.5$. Only a small part of the Tornado was covered because the UNSWIRF aperture had a circular image of 100 arcsec in diameter with a pixel size of 0.77 arcsec. The UNSWIRF field of view is marked with a circle in Figure 1. Five frames at different Fabry-Perot settings were obtained in the $2.12 \mu\text{m}$ H₂ 1–0 S(1) line, equally spaced by 40 km s^{-1} and centred on the maser velocity. The velocity resolution of the instrument was $\approx 75 \text{ km s}^{-1}$. The integration time was 180 seconds per frame. For the continuum subtraction, an additional frame was taken at a velocity setting of -400 km s^{-1} from the first frame. A velocity cube, constructed from the five frames, is fitted with the instrumental Lorentzian profile to determine the H₂ line parameters across the field. The H₂ line flux density and line centre velocity are determined to within ≈ 30 per cent and $\approx 20 \text{ km s}^{-1}$, respectively. The intensity was calibrated using additional observations of the standard star BS 8658. To establish the coordinate scale for the UNSWIRF image, we used the *K*-band ($2.15 \mu\text{m}$) stellar positions listed in the Two Micron All Sky Survey (2MASS) point source catalogue¹ (Cutri 1997), which are accurate to 0.1 arcsec.

2.2 SEST observations

We used the 15-m Swedish-ESO Submillimeter Telescope (SEST) during June 2000 to observe the region towards the OH(1720 MHz) maser in ¹²CO, ¹³CO, CS, HCO⁺, HCN and H₂CO transitions between 1.3 and 3 mm. Table 1 lists the observed molecular transitions, frequencies and corresponding telescope beam widths. The spectral resolution ranged between $\approx 0.1 \text{ km s}^{-1}$ at 1.3 mm and $\approx 0.3 \text{ km s}^{-1}$ at 3 mm. The observations were performed in position-switching mode with reference position at RA(1950) =

$17^{\text{h}} 47^{\text{m}} 10^{\text{s}}$, Dec.(1950) = $-32^{\circ} 43' 00''$. The two ¹²CO transitions were obtained over a $2 \times 2 \text{ arcmin}^2$ region centred at RA(1950) = $17^{\text{h}} 36^{\text{m}} 54^{\text{s}}$, Dec.(1950) = $-30^{\circ} 56' 25''$, with a 20 arcsec grid and 30 second integration per position. For the other molecular transitions, observations were taken in a five point-cross grid centred at RA(1950) = $17^{\text{h}} 36^{\text{m}} 54^{\text{s}}$, Dec.(1950) = $-30^{\circ} 56' 05''$, plus 20 arcsec offset. The integration times were 60 seconds for the ¹²CO and ¹³CO transitions and 180 seconds for all the other transitions.

Telescope pointing accuracy to better than 5 arcsec was maintained using periodic observations of the SiO masers associated with AHSco and WHyd. The data have been corrected on-line for atmospheric absorption by periodic observations of a blackbody calibration source. After baseline subtraction and Hanning smoothing, the data were scaled to main-beam brightness temperature (T_{mb}) using the main-beam efficiencies (0.74, 0.70, 0.67 and 0.45 at 85–100 GHz, 100–115 GHz, 130–150 GHz and 220–265 GHz respectively).

2.3 VLA data

The radio continuum data were obtained from archives of the Very Large Array (VLA) of the National Radio Astronomy Observatory (NRAO). The observations of the Tornado nebula were carried out on 28 April 1991 and 13 December 1985 at 20 cm in its A and D-array configurations, respectively. Standard calibration of both data sets used 1748–253 and 3C286 as the phase and amplitude calibrators, respectively. Standard self-calibration was also applied to both data sets before the final image was constructed using the Maximum Entropy method (MEM in AIPS).

3 RESULTS AND ANALYSIS

The 20 cm radio image of Tornado, shown in Figure 1, has a resolution of $2.65'' \times 1.07''$ (PA= -6.7°). The image illustrates nebula’s filamentary structure and we indicate the main features – the bright western region is called the ‘Head’, which is followed by a prominent arc in the centre of the nebula and faint filaments comprising the ‘Tail’ of the nebula. The compact source near the nebula, the Eye of the Tornado, is also indicated.

3.1 H₂ emission

We have detected for the first time H₂ line emission towards the Tornado. Figure 2 shows contours of the velocity-integrated $2.12 \mu\text{m}$ H₂ 1–0 S(1) line emission overlaid on a greyscale image of the 2MASS *K*-band ($2.15 \mu\text{m}$). The emission is ring-shaped with a diameter of $\approx 50 \text{ arcsec}$, and contains a number of peaks. The emission peaks are 5–10 arcsec in size. The peak flux density of the $2.12 \mu\text{m}$ H₂ 1–0 S(1) line emission is $1.4 \times 10^{-4} \text{ erg s}^{-1} \text{ cm}^{-2} \text{ sr}^{-1}$ and the 3σ rms noise is $8 \times 10^{-5} \text{ erg s}^{-1} \text{ cm}^{-2} \text{ sr}^{-1}$; the integrated flux density of the whole source is $2.4 \times 10^{-12} \text{ erg s}^{-1} \text{ cm}^{-2}$. After correcting for an assumed extinction in *K*-band of at least $A_K \approx 3$ (since the object is behind the Galactic centre), the peak flux density of the $2.12 \mu\text{m}$ H₂ 1–0 S(1) line emission is $2.2 \times 10^{-3} \text{ erg s}^{-1} \text{ cm}^{-2} \text{ sr}^{-1}$, the integrated flux density is $3.8 \times 10^{-11} \text{ erg s}^{-1} \text{ cm}^{-2}$, and the $2.12 \mu\text{m}$ H₂ luminosity is

¹ see <http://spider.ipac.caltech.edu/staff/hlm/2mass/calvsuc/calvsuc.html> for distance of 11.8 kpc.

The H₂ line centre velocities, marked in Figure 2 span over $\sim 100 \text{ km s}^{-1}$ across the emission region. There are 7 identifiable clumps, with velocities ranging from -95 to $+25 \text{ km s}^{-1}$, with the mean velocity around -54 km s^{-1} . They range from 40 km s^{-1} blue of the mean to 70 km s^{-1} red of the mean. Apart from the clump at $+26 \text{ km s}^{-1}$, however, they are all blue-shifted from the velocity of the cloud, as determined by the CO and OH maser emission. The emission at positive velocities appears as a knot located at the south-eastern region. Unfortunately, this component was not observed with sufficient Fabry-Perot spacings to infer the red-shifted extent of its emission.

3.2 CO emission

Several ¹²CO and ¹³CO emission components at different velocities were detected along the line of sight to the Tornado nebula. Some of the features can be seen in Figure 3, which shows the ¹²CO 1–0 spectrum towards the position of the OH(1720 MHz) maser in the range -40 to $+15 \text{ km s}^{-1}$. In Figure 4 we show the individual ¹²CO 2–1 spectra across a $2 \times 2 \text{ arcmin}^2$ region of the Tornado’s Head. The (0,+20) position corresponds to the location of the OH(1720 MHz) maser. Similarly, Figure 5 shows the five ¹³CO 2–1 spectra, where the (0,0) position corresponds to the location of the OH(1720 MHz) maser. We have assumed that the molecular cloud associated with the Tornado nebula has a velocity close to the maser velocity (-12.4 km s^{-1}), and the spectrum shows a CO feature near -12 km s^{-1} with a linewidth of $\sim 4 \text{ km s}^{-1}$. The spectral features were fitted with Gaussian profiles and the resulting line parameters for the cloud associated with the nebula are summarised in Table 1. In contrast to the ¹²CO and ¹³CO transitions, the other molecular transitions were found to be very weak, providing only upper limits (Table 1). We found no significant line broadening ($\gtrsim 10 \text{ km s}^{-1}$) in the present data which would provide a clear kinematic evidence of shock interaction.

The measured line ratio $R = T_{mb}^{12\text{CO}}/T_{mb}^{13\text{CO}}$ was ≈ 3.4 for the 1–0 transitions, and ≈ 3.0 for the 2–1 transitions, which implies that the ¹²CO emission is optically thick. Adopting an overall isotope ratio $R_I = [^{12}\text{C}/^{13}\text{C}] = 50 \pm 20$ (e.g., Langer & Penzias 1990), we estimate an upper limit on the ¹²CO optical depth of $\tau \approx R_I/R \approx 21$ for the 1–0 line. Since ¹²CO is optically thick, the actual ¹²CO 1–0/2–1 line ratio should be close to unity. Thus, by equating the two brightness temperature of the two ¹²CO lines, we derived a beam-deconvolved source size of $\approx 40 \text{ arcsec}$. We can then calculate the actual brightness temperatures corrected for the source size from $T_S = T_{mb}(1 + \Omega_B/\Omega_S)$, where Ω_B and Ω_S are the beam and source solid angles, respectively (e.g., Jansen, van Dishoeck & Black 1994; Rohlfs & Wilson 1996). For the two ¹²CO transitions we then have $T_S(1 - 0) = 20 \text{ K}$ and $T_S(2 - 1) = 14 \text{ K}$. To determine the temperature of the molecular gas towards the ¹²CO peak, we used the molecular-line excitation code with the mean escape probability (MEP) (for details see e.g., Jansen et al. 1994). Our excitation modeling of the two ¹²CO lines implies a kinetic temperature of $20 \pm 5 \text{ K}$ for a gas density of 10^4 – 10^6 cm^{-3} . This is consistent with the fact that for an optically thick ¹²CO the gas temperature should be similar to the brightness tempera-

ture of the ¹²CO lower-energy transitions. We also estimate ¹²CO column density of $N(^{12}\text{CO}) \approx (1 - 8) \times 10^{17} \text{ cm}^{-2}$ from our modeling. Using the standard fractional abundance [¹²CO]/[H₂] of 10^{-4} (e.g., Irvine, Goldsmith, & Hjalmarson 1987; van Dishoeck, Jansen, & Phillips 1993) we derive $N(\text{H}_2) \approx (1 - 8) \times 10^{21} \text{ cm}^{-2}$. The upper limit of the ¹³CO optical depth is $24/70 = 0.3$, and column density is $2.7 \times 10^{16} \text{ cm}^{-2}$. Because of the non-detection of molecules with larger dipole moments (e.g., CS), we do not have a more reliable method to constrain the density of the molecular gas.

A velocity-integrated map of ¹²CO 2–1 emission between -10 and -16 km s^{-1} is shown in Figure 6. Since the optical depths are large, the observed ¹²CO distribution traces the temperature distribution rather than the column density distribution.

4 DISCUSSION

H₂ emission has been studied in only a few of the known SNR masers, such as IC 443 (Burton et al. 1988), Sgr A East (Yusef-Zadeh et al. 2001) and G359.1–0.5 (Lazendic et al. 2002). The line ratio of the H₂ 1–0 and 2–1 S(1) transitions may be used to establish the excitation mechanism for H₂ emission. Unfortunately, we were unable to obtain 2–1 S(1) observations towards the Tornado, but we argue on the basis of morphology and kinematics that the H₂ emission detected towards the OH(1720 MHz) maser in the Tornado nebula is shock excited, as found in other SNR associated with OH(1720 MHz) emission (e.g., Burton et al. 1988; Lazendic et al. 2002, 2004). In Figure 7 we compare the integrated $2.12 \mu\text{m}$ H₂ 1–0 S(1) line emission with the 20 cm radio continuum emission. In the region where the SNR encounters a dense molecular cloud the SNR shock will be decelerated, producing enhanced radio emission due to strong shock compression and enhanced particle acceleration. Both the H₂ and radio continuum emission features have filamentary morphology, and there is a good correlation between the H₂ and radio continuum maxima; we interpret this agreement as an indication of physical association. The bright clumps in the H₂ emission represent small-scale structures in the inhomogeneous ambient medium, illuminated by the SNR shock (see e.g., Burton et al. 1988). Another argument for shock excitation is the significant velocity motion in the H₂ emitting gas across the region, which is opposite to that found in fluorescent sources where velocities are essentially at the ambient velocity of the molecular cloud (Burton, Hollenbach, & Tielens 1990). The H₂ emission is also spatially coincident with extended OH(1720 MHz) emission found towards the nebula (Yusef-Zadeh et al. 1999), which is believed to be evidence of large-scale interactions between a SNR and an adjacent molecular cloud.

The molecular cloud associated with the nebula and the OH(1720 MHz) maser is optically thick, with a kinetic temperature of $\approx 20 \text{ K}$ and a gas density of 10^4 cm^{-3} . This temperature and density are in agreement with properties expected for the molecular cloud interacting with SNRs associated with OH(1720 MHz) masers (Lockett et al. 1999), which suggests that we are detecting mostly the pre-shock molecular gas. We did not detect the broad line profiles from the warm post-shock region, like those seen in

IC 443 (van Dishoeck et al. 1993). The 50 arcsec diameter of the H₂ ring is comparable to the 45 arcsec beam size at the ¹²CO 1–0 frequency, and we might expect to detect the warm shocked gas. Indeed, the location of the OH(1720 MHz) maser within the CO peak contour in Figure 6 indicates that we might detect contribution from both the pre-shock and post-shock gas. However, the molecular gas is optically thick and we might be probing only the cool envelope of the cloud with the observations of the ¹²CO transitions. Furthermore, weaker broad wings from the warm gas might be confused with neighbouring molecular features. Similar observations of shocked molecular gas towards other SNRs imply that the broad emission component is usually stronger in higher ¹²CO transitions (e.g., Seta et al. 1998), or restricted to a small molecular clumps (e.g., Reach et al. 2002). Thus, observations of higher energy transitions (which would also result in higher spatial resolution) might be needed to detect the shocked molecular gas in the millimetre band. Indeed, preliminary results from observations of CO 4–3 line show broad line emission centered at -12 km s^{-1} (Yusef-Zadeh et al. 2004, in preparation).

Figure 8a shows the integrated ¹²CO 2–1 line emission superimposed on the 20 cm radio continuum emission. The blast wave delineated by the radio emission is indented at the location of the OH(1720 MHz) maser and the ¹²CO peak, suggesting that the molecular cloud is large and dense enough to cause a significant impediment to the shock front. This resembles the well known case of SNR-cloud interaction seen in the Cygnus Loop (e.g., Danforth, Blair, & Raymond 2001). Also, the western side of the H₂ emission appears more flattened compared to the other parts, which is suggestive of a compression resulting from the interaction between the nebula and the surrounding molecular gas. Thus, the OH(1720 MHz) maser, the H₂ emission and the radio continuum indentation is the indication that the blast wave has just begun to interact with the tip of the molecular cloud. The distribution of molecular gas components is consistent with the OH(1720 MHz) maser being located in a post-shock layer just behind a shock front, oriented transverse to the line of sight, as predicted by the theory for OH(1720 MHz) maser formation (Elitzur 1976; Lockett et al. 1999). Furthermore, the X-ray flux observed from the Tornado (Gaensler et al. 2003) is consistent with that required to produce the necessary OH (Wardle 1999).

The OH(1720 MHz) maser is located at the western edge of the H₂ emission and its velocity (-12 km s^{-1}) differs significantly from the mean velocity of H₂ emission. This is not too surprising because we see masers only at the location where the shock is propagating perpendicular to our line of sight (Lockett et al. 1999), whereas we see H₂ emission from any location in the shocked gas. The extended maser emission spans over a larger velocity gradient between -13.1 and -8.7 km s^{-1} (Yusef-Zadeh et al. 1999). It is expected that the shock associated with extended maser emission is not exactly perpendicular to the line of sight, although these velocities are still much lower than the mean velocity of H₂ emission. The large velocity span of H₂ emission features is probably the result of seeing a shock under different angles. Although H₂ emission appears ring-like, the distribution of H₂ line-velocities, when compared to -12 km s^{-1} as a reference, is clearly incompatible with any expansion of a ring. In fact, it may be simply a chance line of sight projection

that is causing the apparent ring structure. Presumably the north-west structure of the H₂ ring is marking the shock front as it runs into the CO cloud, given the position offset between the CO and H₂ in Figure 8b. The rest of the H₂ ring is probably not a continuous structure but foreground or background structure being shocked with a different shock velocity vector. This is supported by the fact that there is no coherence between clumps in velocity between two adjacent clumps at different velocities when we examine the H₂ cube, and velocities jump from one clump to the other supporting the notion that clumps are distinct features. If we suppose the greatest shock speed is V_{max} , running in to the lowest density molecular gas, n_{min} , then the line of sight velocity we measure is $V = V_{max}(n_{min}/n)^{0.5} \cos(\theta)$, where the velocity V is with respect to the -12 km s^{-1} ambient cloud value, with $\theta = 90^\circ$ being the plane of the sky, and n is the density at that point. In general the velocities get more negative towards the rear of the ring, which implies that θ is small here so the shock is moving nearly directly towards us to the rear of the H₂ ring.

5 SUMMARY

We have detected 2.12 μm H₂ 1–0 S(1) emission towards the northwestern edge of the Tornado nebula. The emission has a ring-like morphology and encompasses the location of the OH(1720 MHz) maser. The correlation between the radio continuum and H₂ emission, and significant velocity motions suggest that the H₂ emission originates from an expansion of the shock wave and is most probably shock excited. The OH(1720 MHz) maser is located at the western edge of the H₂ emission, which probably delineates the leading edge of shock front.

Molecular transitions of ¹²CO and ¹³CO were also detected at the maser velocity of -12 km s^{-1} ; emission from CS, HCO⁺, HCN and H₂CO was not detected. The millimetre-line observations were found to probe only the ambient molecular gas associated with the nebula, which is optically thick, warm ($\approx 20 \text{ K}$) and dense ($\gtrsim 10^4 \text{ cm}^{-3}$). The location of the molecular gas coincides with an indentation in the radio continuum distribution and the OH(1720 MHz) maser position, suggesting that the molecular cloud is large enough to cause significant deceleration of the blast wave shock. Observations of optically thinner higher transitions of ¹²CO are needed to examine the properties of shocked part of the molecular gas.

6 ACKNOWLEDGMENTS

We thank John Black for kindly providing us with his MEP code. JSL was supported by an Australian Government International Postgraduate Research Scholarship, a Sydney University Postgraduate Scholarship, and an ATNF Postgraduate Scholarship. JSL also acknowledges travel support from the Australian Government’s Access to Major Research Facilities Program.

The NIR observations would not have been possible without the efforts of Michael Ashley and the UNSWIRF crew from UNSW, as well as the staff of the Anglo Australian Observatory. The Swedish-ESO Submillimetre Tele-

scope (SEST) is operated by the Swedish National Facility for Radio Astronomy, Onsala Space Observatory and by the European Southern Observatory (ESO). The National Radio Astronomy Observatory (NRAO) is a facility of the National Science Foundation, operated under a cooperative agreement by Associated Universities, Inc. This publication makes use of data products from the Two Micron All Sky Survey (2MASS), which is a joint project of the University of Massachusetts and the Infrared Processing and Analysis Center/California Institute of Technology, funded by the National Aeronautics and Space Administration and the National Science Foundation.

REFERENCES

- Brogan, C. L. & Goss, W. M. 2003, *AJ*, 125, 272
 Becker, R. H. & Helfand, D. J. 1985, *Nature*, 313, 115
 Brogan, C. L., Frail, D. A., Goss, W. M., & Troland, T. H. 2000, *ApJ*, 537, 875
 Burton, M. G., Geballe, T. R., Brand, P. W. J. L., & Webster, A. S. 1988, *MNRAS*, 231, 617
 Burton, M. G., Hollenbach, D. J., & Tielens, A. G. G. M. 1990, *ApJ*, 365, 620
 Burton, M. G., Lazendic, J. S., Yusef-Zadeh, F., & Wardle, M. 2004, *MNRAS*, 348, 638
 Caswell, J. L., Haynes, R. F., Milne, D. K., & Wellington, K. J. 1980, *MNRAS*, 190, 881
 Caswell, J. L., Kesteven, M. J., Bedding, T. R., & Turtle, A. J. 1989, *Proceedings of the Astronomical Society of Australia*, 8, 184
 Clark, D. H. & Caswell, J. L. 1976, *MNRAS*, 174, 267
 Cutri, R. M. 1997, in *The Impact of Large Scale Near-IR Sky Surveys*, ed. F. Garzón et al. (Dordrecht: Kluwer), 187
 Danforth, C. W., Blair, W. P., & Raymond, J. C. 2001, *AJ*, 122, 938
 Elitzur, M. 1976, *ApJ*, 203, 124
 Gaensler, B. M., Fogel, J. K. J., Slane, P. O., Miller, J. M., Wijnands, R., Eikenberry, S. S., & Lewin, W. H. G. 2003, *ApJL*, 594, L35
 Fich, M., Blitz, L., & Stark, A. A. 1989, *ApJ*, 342, 272
 Frail, D. A., Goss, W. M., Reynoso, E. M., Giacani, E. B., Green, A. J., & Otrupcek, R. 1996, *AJ*, 111, 1651
 Green, A. J., Frail, D. A., Goss, W. M., & Otrupcek, R. 1997, *AJ*, 114, 2058
 Helfand, D. J. & Becker, R. H. 1985, *Nature*, 313, 118
 Irvine, W. M., Goldsmith, P. F., & Hjalmarson, A. 1987, *ASSL Vol. 134: Interstellar Processes*, 561
 Jansen, D. J., van Dishoeck, E. F. & Black, J. H. 1994, *A&A*, 282, 605
 Langer, W. D. & Penzias, A. A. 1990, *ApJ*, 357, 477
 Lazendic, J. S., Wardle, M., Burton, M. G., Yusef-Zadeh, F., Whiteoak, J. B., Green, A. J., & Ashley, M. C. B. 2002, *MNRAS*, 331, 537
 Lazendic, J. S., Wardle, M., Whiteoak, J. B., Burton, M. G. & Green, A. J., 2004, to be submitted to *MNRAS*
 Lockett, P., Gauthier, E. & Elitzur, M. 1999, *ApJ*, 511, 235
 Manchester, R. N. 1987, *A&A*, 171, 205
 Milne, D. K. 1979, *Australian Journal of Physics*, 32, 83
 Radhakrishnan, V., Goss, W. M., Murray, J. D., & Brooks, J. W. 1972, *ApJS*, 24, 49
 Reach, W. T., Rho, J., Jarrett, T. H., & Lagage, P. 2002, *ApJ*, 564, 302
 Rohlfs, K. & Wilson, T. L. 1996, *Tools of Radio Astronomy*, Springer-Verlag, Berlin
 Ryder, S. D., Sun, Y.-S. Ashley, M. C. B., Burton, M. G., Allen, L. E. & Storey, J. W. V. 1998, *Publications of the Astronomical Society of Australia*, 15, 228
 Seta, M. et al. 1998, *ApJ*, 505, 286
 Shaver, P. A., Salter, C. J., Patnaik, A. R., van Gorkom, J. H., & Hunt, G. C. 1985, *Nature*, 313, 113
 Shaver, P. A., Pottasch, S. R., Salter, C. J., Patnaik, A. R., van Gorkom, J. H., & Hunt, G. C. 1985, *A&A*, 147, L23
 Shull, J. M., Fesen, R. A., & Saken, J. M. 1989, *ApJ*, 346, 860
 Stewart, R. T., Haynes, R. F., Gray, A. D., & Reich, W. 1994, *ApJL*, 432, L39
 van Dishoeck, E. F., Jansen, D. J., & Phillips, T. G. 1993, *A&A*, 279, 541
 Wardle, M. 1999, *ApJL*, 525, L101
 Wardle, M. & Yusef-Zadeh, F. 2002, *Science*, 296, 2350
 Weiler, K. W. & Panagia, N. 1980, *A&A*, 90, 269
 Yusef-Zadeh, F., Goss, W. M., Roberts, D. A., Robinson, B., & Frail, D. A. 1999, *ApJ*, 527, 172
 Yusef-Zadeh, F., Stolovy, S. R., Burton, M., Wardle, M., & Ashley, M. C. B. 2001, *ApJ*, 560, 749
 Yusef-Zadeh, F., Wardle, M., Rho, J., & Sakano, M. 2003, *ApJ*, 585, 319

Table 1. Molecular lines observed towards the Tornado nebula at RA(1950) = 17^h 36^m 54^s, Dec.(1950) = -30° 56' 05". The first three columns list the molecular transitions and their frequencies. The fourth column lists the SEST beam sizes (FWHM), and the last three columns give the spectral-line parameters: main-beam brightness temperature (T_{mb}) and rms noise (upper limits are 2σ values), central velocity (V_{LSR}) and line width (ΔV_{LSR}).

Molecule	Transition	ν (GHz)	Beam Size (arcsec)	T_{mb} (K)	V_{LSR} (km s ⁻¹)	ΔV_{LSR} (km s ⁻¹)
¹² CO	2-1	230.538	23	10.5±0.3	-11.0	4.0
	1-0	115.271	45	8.6±0.4	-11.2	5.1
¹³ CO	2-1	220.399	23	3.5±0.2	-11.0	3.7
	1-0	110.201	45	2.5±0.1	-11.1	3.7
CS	3-2	146.969	34	<0.1	-	-
	2-1	97.981	52	<0.2	-	-
HCO ⁺	1-0	89.188	54	<0.2	-	-
HCN	1-0	88.632	55	<0.1	-	-
H ₂ CO	3 _(2,2) -2 _(2,1)	218.475	23	<0.1	-	-
	3 _(0,3) -2 _(0,2)	218.222	24	<0.1	-	-

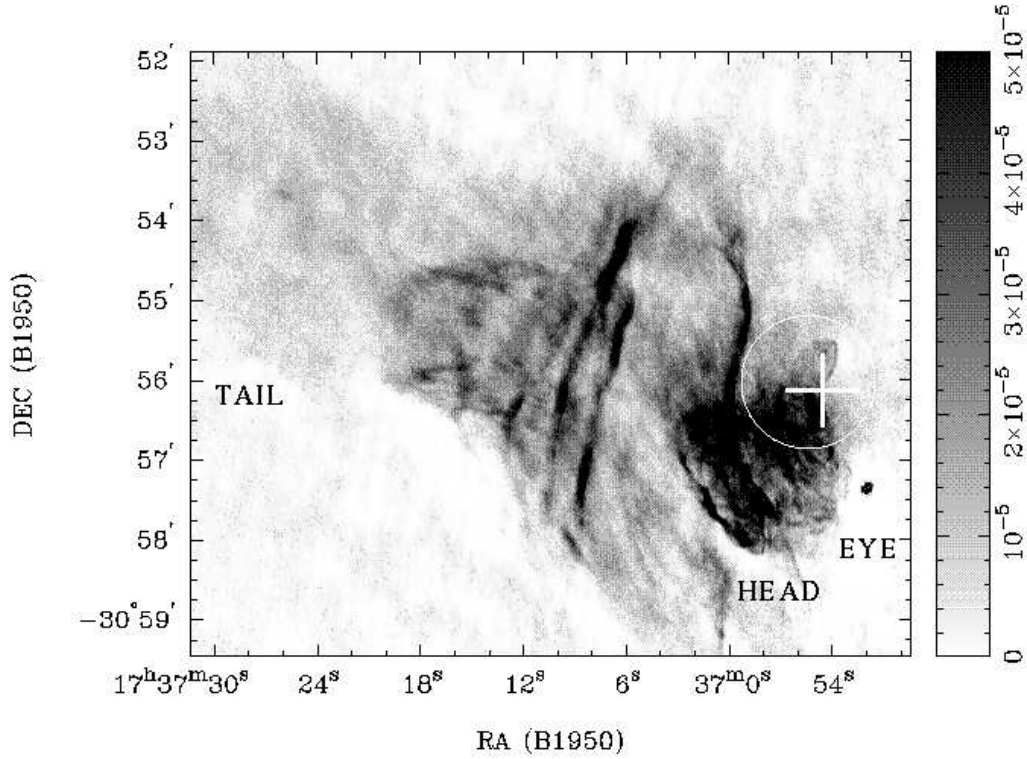


Figure 1. 20 cm Very Large Array image of the Tornado nebula with the main features labelled. The cross marks the location of the OH(1720 MHz) maser and the circle marks the field of view of the UNSWIRF aperture (see Section 2.1).

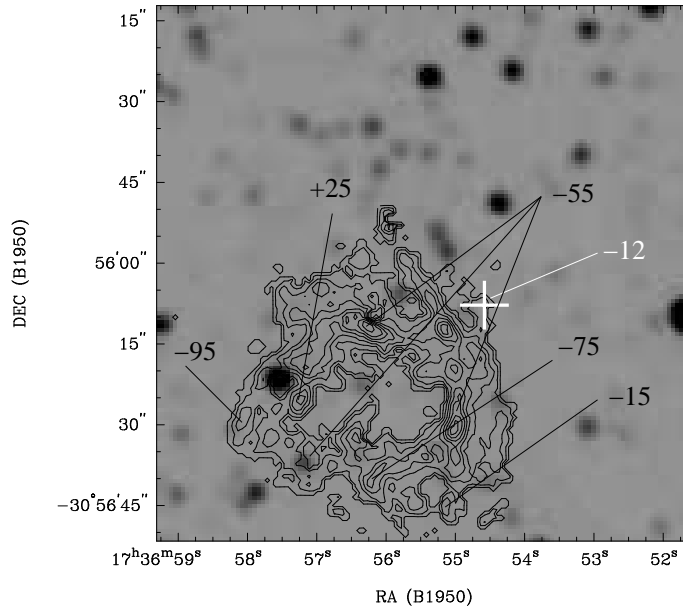


Figure 2. Contours of the velocity-integrated $2.12 \mu\text{m}$ H_2 1-0 S(1) line emission towards the OH(1720 MHz) maser in the Tornado nebula, overlaid on the 2MASS K-band greyscale image matching the size of the UNSWIRF field of view. The contours are: 1.6, 4.7, 6.3, 7.9, 9.5, 11.1, 12.6, $14.2 \times 10^{-5} \text{ erg s}^{-1} \text{ cm}^{-2} \text{ sr}^{-1}$. The white cross marks the location (and the velocity) of the OH(1720 MHz) maser. Labelled are also the line centre velocities (in km s^{-1}) of prominent features.

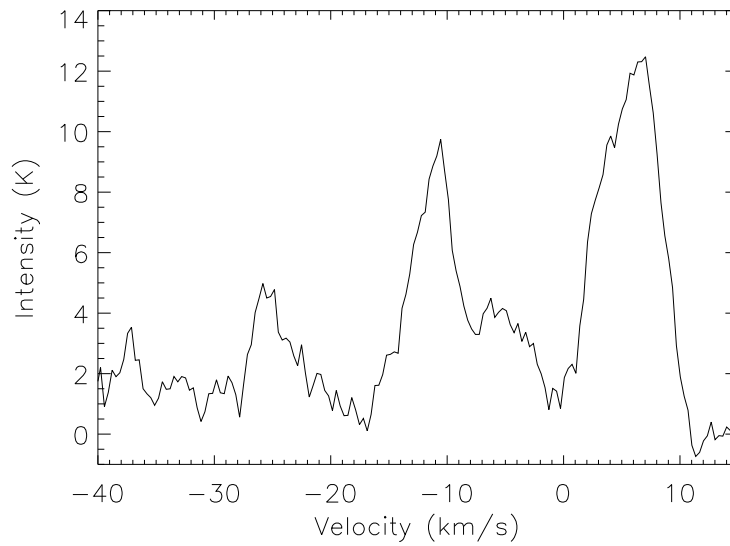


Figure 3. ^{12}CO 1–0 spectrum observed towards the OH(1720 MHz) maser in the Tornado nebula in the range -40 to $+15$ km s^{-1} demonstrates spectral features along the line of sight.

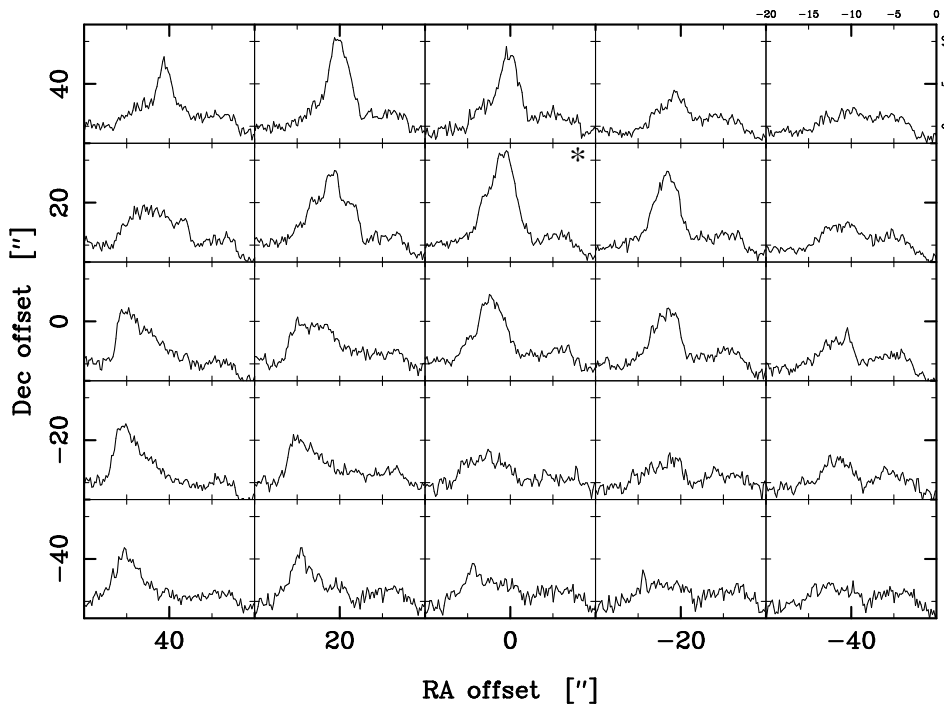


Figure 4. ^{12}CO 2–1 spectra taken over $2'' \times 2'$ region towards the OH(1720 MHz) maser in the Tornado nebula. The (0,0) position is at RA(1950) = $17^{\text{h}} 36^{\text{m}} 54^{\text{s}}$, Dec.(1950) = $-30^{\circ} 56' 25''$, and the spectrum closest to the OH(1720 MHz) masers position is marked with a star. The scale is given in the panel in the upper right; the velocity and temperature scales are given in K and km s^{-1} , respectively.

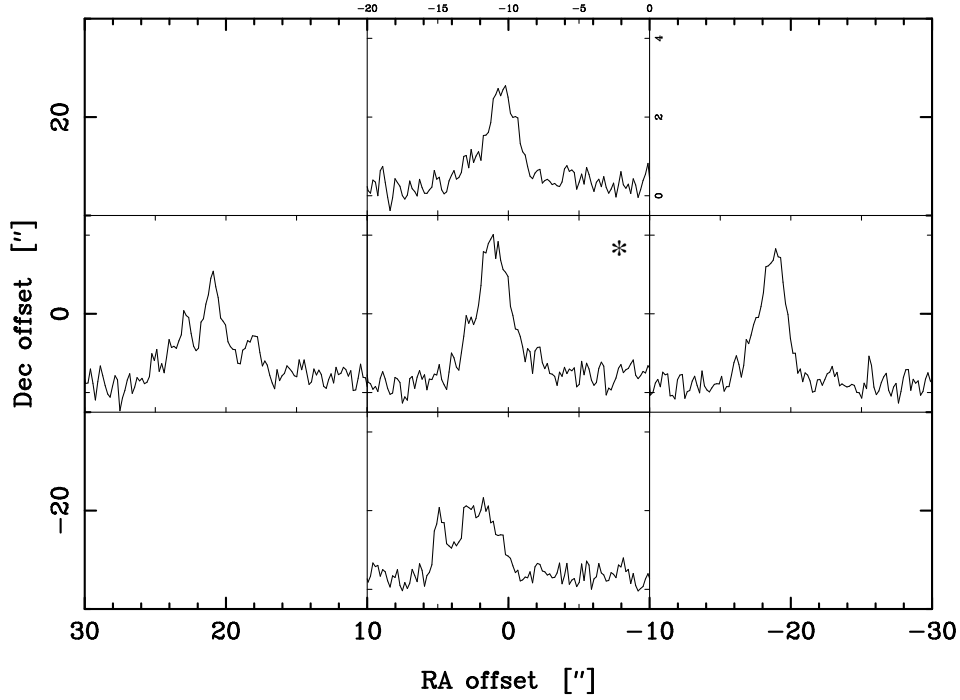


Figure 5. ^{13}CO 2–1 spectra taken over $2'' \times 2''$ region towards the OH(1720 MHz) maser in the Tornado nebula. The (0,0) position is at RA(1950) = $17^{\text{h}} 36^{\text{m}} 54^{\text{s}}$, Dec.(1950) = $-30^{\circ} 56' 05''$, and the spectrum closest to the OH(1720 MHz) masers position is marked with a star. The scale is given in the upper panel; the velocity and temperature scales are given in K and km s^{-1} , respectively.

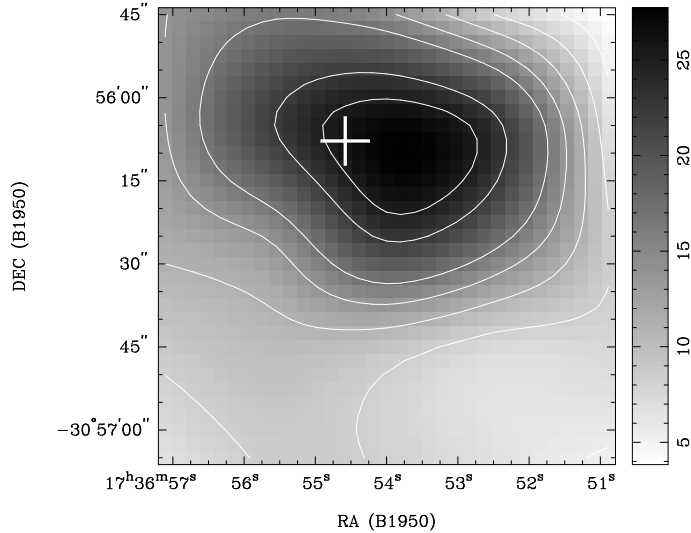


Figure 6. Integrated ^{12}CO 2–1 emission towards OH(1720 MHz) maser in the Tornado. The contours are: 8, 11, 14, 17, 22 and 25 K km s^{-1} . The cross marks the location of the OH(1720 MHz) maser.

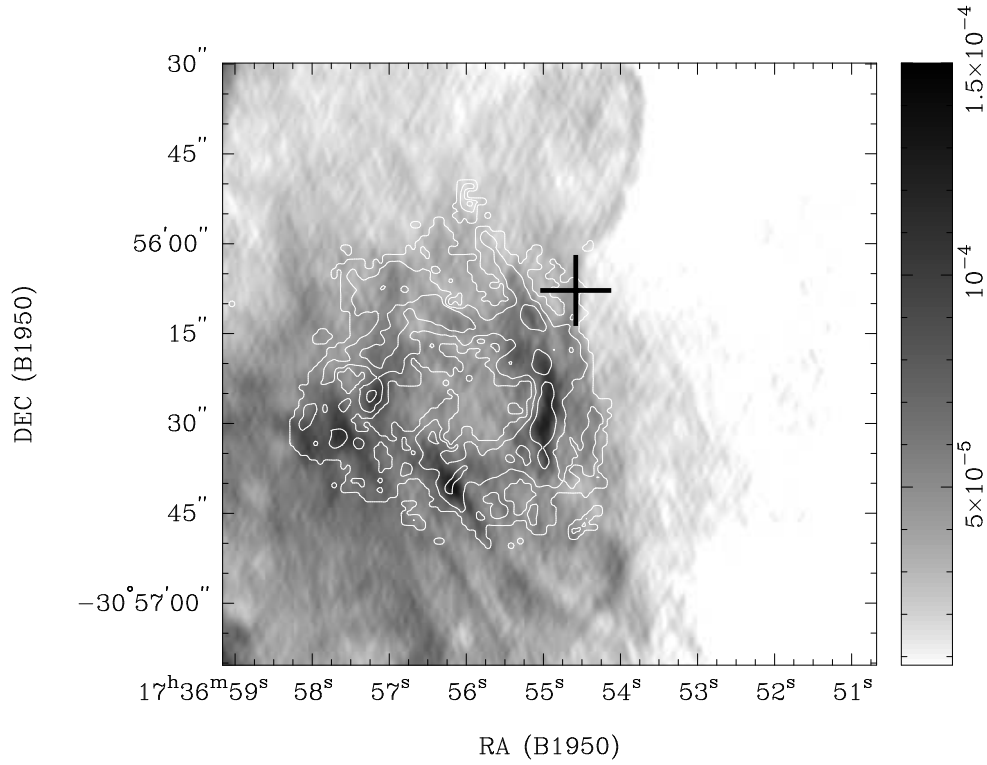


Figure 7. Contours of H₂ 1–0 S(1) line emission superimposed on the 20 cm VLA grayscale image. The contour levels are 1.6, 6.3 and 9.5×10^{-5} $\text{erg s}^{-1} \text{cm}^{-2} \text{sr}^{-1}$. The cross marks the location of the OH(1720 MHz) maser.

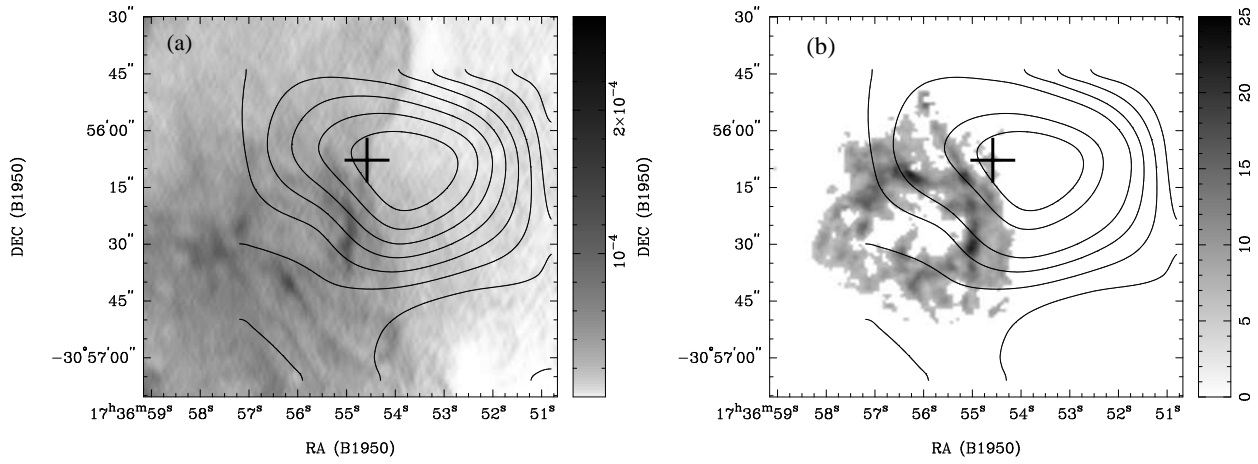


Figure 8. Contours of the ¹²CO 2–1 line emission overlaid on (a) the 20 cm grayscale VLA image and (b) the velocity-integrated 2.12 μm H₂ 1–0 S(1) line emission in the Tornado nebula. The ¹²CO contours are the same as in Figure 6. The cross marks the location of the OH(1720 MHz) maser.